machines

MDPI

Article

Pareto Analysis of Electro-Mechanical Variables in Predictive Control of Drives

Manuel G. Satué †, Manuel R. Arahal *,† and Manuel G. Ortega

Departamento de Ingeniería de Sistemas y Automática, Universidad de Sevilla, E-41092 Seville, Spain
* Correspondence: arahal@us.es
† These authors contributed equally to this work.

Abstract: Variable speed drives are often controlled by a double-loop scheme in which a proportional integral controller takes on the speed loop. The tuning of this loop is a complex job. In most cases just mechanical variables are considered for tuning. This paper presents a new Pareto analysis incorporating mechanical and electrical variables. A state of the art finite state model predictive controller is used for stator current control. The analysis is performed using experimental data from a five-phase induction motor and considers considering commonly found performance indicators derived from experimental data. The results show undocumented connections between those performance indicators. The analysis not only helps in PI tuning but, more importantly, prompts for a revision of the methods usually utilized to report performance enhancements of new methods.

Keywords: multiphase system; PI tuning; predictive control; variable speed drive

check for updates

Academic Editor: Antonio J. Marques Cardoso

Received: 16 December 2024
Revised: 24 January 2025
Accepted: 9 February 2025
Published: 15 February 2025

Citation: Satué, M.G.; Arahal, M.R.; Ortega, M.G. Pareto Analysis of Electro-Mechanical Variables in Predictive Control of Drives. *Machines* **2025**, *13*, 150. https://doi.org/10.3390/machines13020150

Copyright: © 2025 by the authors. Licensee MDPI, Basel, Switzerland. This article is an open access article distributed under the terms and conditions of the Creative Commons Attribution (CC BY) license (https://creativecommons.org/licenses/by/4.0/).

1. Introduction

Variable speed drives often use a double control loop where the outer one is devoted to mechanical speed and the inner one to stator current control [1]. The current loop is much faster requiring action on the Voltage Source Inverter (VSI) about every 50 microseconds [2]. This regulates the motor currents which, in turn, produce a torque to manage the mechanical speed [3]. Recently, Finite State Model Predictive Control (FSMPC) has been proposed for current control, which does not require modulation such as PWM, instead the VSI state is directly set by the inner controller [4]. This has been reported as providing a high bandwidth control of stator currents, benefiting the drive operation [5,6]. In FSMPC, the control signal is derived from the optimization of a cost function (CF). The problem of tuning, however, was still an issue. In particular, tuning of the Weighting Factors (WF) of the FSMPC needs some work.

In FSMPC, the interaction of the interior loop with the speed loop is conducted following the Indirect Field Oriented Control (IFOC) scheme. The method requires an approximate knowledge of the time constant of the rotor circuit to ensure stability [7,8]. Following these works, some variations have appeared for sensorless operation [9] and other variations [10]. However, in most cases, the underlying models do not include non-idealities such as nonlinear behavior of the motor, VSI+modulation behavior and mechanical speed sensing via incremental encoders [11,12].

In the absence of better models, for instance, the inclusion of non-idealities, researchers and practitioners have turned to the experimental approach for controller tuning. Meta-heuristic optimisation algorithms [13], fuzzy [14] and neural approaches [15] are some of the proposed techniques reported in the literature. These mostly rely on data but do not provide insight regarding trade-offs.

One particular type of machine that has received particular attention is multi-phase motors. However, it has been reported that their intrinsic advantages are somehow hindered by increased complexity, but their combination with FSMPC has made them more attractive. Prior to this accumulative approach, the interaction among phases made tuning more complex, requiring four proportional integral (PI) controllers and a modulation such as PWM [16]. The decomposition of stator currents into a torque related space ($\alpha - \beta$) and several harmonic spaces ($x_j - y_j$, $j \geq 1$) is a challenge for control design [17]. The number of phases makes each case different. However, for FSMPC the same simple structure can be used for any number of phases [18], and, in general, its flexibility goes beyond that. For instance, some new modulation schemes are now possible [19,20]. In addition, multi-phase systems offer better fault-tolerant possibilities [21]. However, its flexibility comes at the price of higher dependence on the model [22] and the need for tuning of the weighting factors (WF).

These new developments can potentially affect the tuning of the outer loop. However, some aspects have proven difficult to model and later treat. For instance, the delay introduced by VSI modulation [23], results in saturation of some variables, delay and ripple in the speed sensing from incremental encoders, etc.

In addition to the above information, some performance indicators lay somehow between the mechanical and the electrical realms. This is the case of the torque ripple [13], which plays an important role in applications for performance and maintenance issues [24]. However, it is disregarded by most studies dealing with tuning of the outer loop. This is motivated by the lack of equations to connect this figure of merit with the outer loop control parameters that would allow other tuning options [25].

In this context, herein, we propose a new Pareto analysis incorporating mechanical and electrical variables. The analysis seeks links or trade-offs between performance indicators as previously desribed in [26–28]. Without this, it can be argued that, the relative merits of any tuning are obscured. A reduction in the set of performance indicators is proposed for outer loop assessment. This set is computed for different tunings so as to obtain an approximation for the Pareto front by means of removing the dominated solutions. This establishes a base-line against which any proposed enhancement should be contrasted.

The structure of the rest of the paper is as follows. The next section introduces the control structure for multiphase drives considered in the analysis. The experimental setup is then presented in Section 3. In Section 4, the discussion of the results is presented. Section 5 ends this paper.

2. Materials and Methods

Pareto analysis uses experimental data obtained from predictive control of a variable-speed drive. The materials used are presented below. The main methods require explanation are related to the control structure and data-gathering processes. These are presented in Sections 2.2–2.4.

2.1. Experimental Setup

The methodology for Pareto analysis consists of gathering data from an experimental setup. The setup is a test-bed for variable-speed drive control. Its main elements are listed below.

- A five-phase Induction Machine that is fed by a voltage source inverter.
- A five-phase VSI that has been custom-made using two SKS 22F modules (SEMIKRON DANFOSS, Nürnberg, Bayern, Germany).
- Hall effect sensors LH25-NP for stator currents (LEM, Geneva, Switzerland).

- An optical encoder coupled to the rotating shaft of the machine from which velocity estimates are obtained. These estimates are used in the IFOC scheme to control the mechanical speed of the IM.
- A TMS320F28335 (Texas Instruments, Dallas, TX, USA) digital signal processor that contains the control program.
- A direct current (DC) motor that is coaxial with the induction motor and capable of producing an opposing torque. This allows the introduction of a load to the system.

These elements are connected via the method shown in Figure 1, where a diagram with photographs is shown. Also, Table 1 provides the parameters for the induction motor. These parameters are needed for the predictive model.

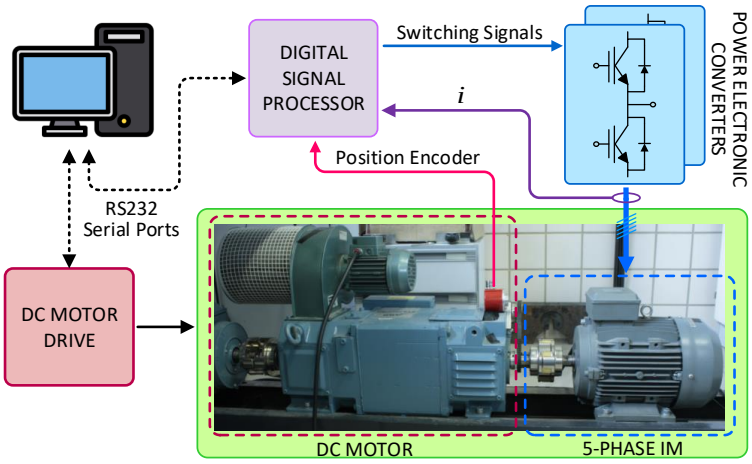


Figure 1. Diagram and photographs of the laboratory setup used in the experiments.

Table 1. Values for the five-phase motor parameters.

Parameter	Value	Unit
Stator resistance, R_s	12.85	Ω
Rotor resistance, R_r	4.80	Ω
Stator leakage inductance, L_{ls}	79.93	mH
Rotor leakage inductance, L_{lr}	79.93	mH
Mutual inductance, L_M	681.7	mH
Rotational inertia, J_m	0.02	kg m^2
Number of pairs of poles, P	3	-
Direct current voltage V_{DC}	300	V
Rated current I_n	2.5	A
Rated power P_n	1000	W

In addition to these elements, the methodology for data gathering is presented below. In particular, the following procedures are explained: the method for drive control, the method for stator current control, and the figures of merit used in Pareto analysis.

2.2. Drive Control

The control scheme using a PI for speed control and FSMPC for stator current control is presented in Figure 2. The outer loop (speed) uses a PÌ as the controller for the mechanical speed (ω). The inner loop uses a predictive block to the control stator current (i_s). The structure is derived from the IFOC scheme, providing independent control of the rotor flux and torque. The reference value for the rotor flux is used to derive current i_d^* that magnetizes the motor. The value for quadrature current i_q^* directly controls the torque. Its reference value is computed by the speed PI as follows:

$$i_q^* = k_p \cdot (\omega^*(t) - \omega^e(t)) + k_i \int_0^\infty (\omega^*(\tau) - \omega^e(\tau))d\tau \tag{1}$$

where ω^* is the set point for speed and ω^e the measured speed.

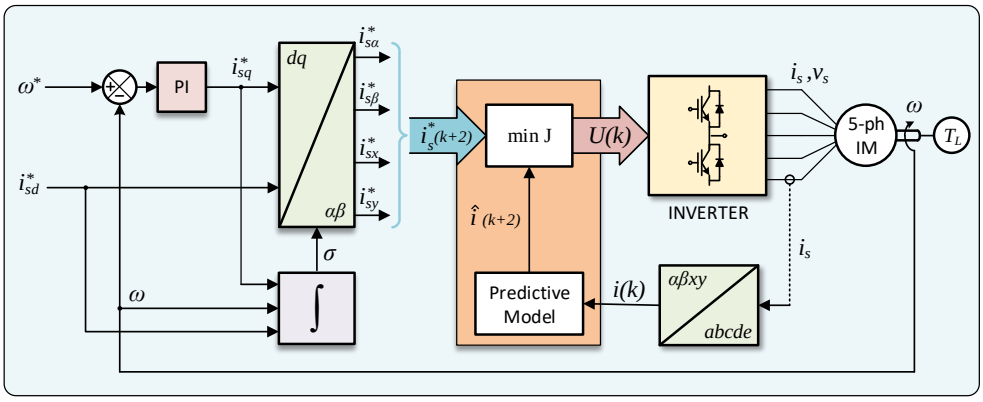


Figure 2. Diagram of the control scheme for a multi-phase motor.

The values in $d-q$ axes are then transformed into $\alpha-\beta$ axes by means of the Park matrix generating

$$I_{\alpha-\beta}^* = D\left(i_d^*, i_q^*\right)^{\mathsf{T}} \tag{2}$$

with

$$D = \begin{pmatrix} \cos\ \theta_a & \sin\ \theta_a \\ -\sin\ \theta_a & \cos\ \theta_a \end{pmatrix} \tag{3}$$

The rotor flux angle θ_a is found as follows

$$\theta_a = \int \omega_e dt,\ \omega_e = \omega_{sl} + P\omega, \tag{4}$$

where

$$\omega_{sl} = \frac{i_q}{i_d}\frac{1}{\hat{\tau}_r} \tag{5}$$

where $\hat{\tau}_r$ is an approximation to the time constant of the rotor circuit

$$\tau_r = L_r/R_r. \tag{6}$$

The inner loop uses a reference current $i^*(k)$ whose amplitude is found as

$$I^* = \sqrt{i_d^{*2} + i_q^{*2}} \tag{7}$$

Finally, the $\alpha-\beta$ reference trajectories are found as

$$i_\alpha^*(t) = I^* \sin\omega_e t,\ i_\beta^*(t) = I^* \cos\omega_e t \tag{8}$$

2.3. Current Loop

Tracking the stator currents is performed by FSMPC following the usual MPC practice. First, the motor model is used to predict future values of the stator currents. Each VSI state

produces a value for stator voltages $v_s(t)$. These are linked to electrical variables and are described as follows:

$$\begin{aligned} v_{\alpha\beta s}(t) &= R_s i_{\alpha\beta s}(t) + \frac{d}{dt}\Psi_{\alpha\beta s}(t) \\ 0 &= R_r i_{\alpha\beta r}(t) + \frac{d}{dt}\Psi_{\alpha\beta r}(t) - j\omega_r(t)\Psi_{\alpha\beta r}(t) \\ \Psi_{\alpha\beta s}(t) &= L_s i_{\alpha\beta s}(t) + L_m i_{\alpha\beta r}(t) = L_s i_{\alpha\beta s}(t) + L_m i_{\alpha\beta r}(t) \\ \Psi_{\alpha\beta r}(t) &= L_m i_{\alpha\beta s}(t) + L_r i_{\alpha\beta r}(t) = L_m i_{\alpha\beta s}(t) + L_r i_{\alpha\beta r}(t) \\ v_{xys}(t) &= R_s i_{xys}(t) + \frac{d}{dt}\Psi_{xys}(t) \\ \Psi_{xys}(t) &= L_{ls} i_{xys}(t) \end{aligned} \tag{9}$$

where the variables used are fluxes $\Psi_s(t)$, $\Psi_r(t)$, currents $i_s(t)$, $i_r(t)$, and electrical speed $\omega_r(t)$. The model also contains parameters identified from the motor, such as inductances L_s, L_r, L_{ls}, L_m, and resistances R_s, R_r. These parameters are provided in Table 1.

The stator voltages depend on V_{DC} (DC link voltage) and the state K_j of VSI switches. Considering the state as a vector $u = (K_1, ..., K_5) \in \boldsymbol{B}^5$ with $\boldsymbol{B} = \{0, 1\}$, then stator voltages $v_{\alpha\beta xys}$ are found as follows:

$$v_{\alpha\beta xys} = (v_{\alpha s}, v_{\beta s}, v_{xs}, v_{ys}) = V_{DC} u TM \tag{10}$$

where TM is given as

$$TM = \begin{pmatrix} a & b & b & b & b \\ b & a & b & b & b \\ b & b & a & b & b \\ b & b & b & a & b \\ b & b & b & b & a \end{pmatrix} \cdot \begin{pmatrix} d & \gamma_1^c & \gamma_2^c & \gamma_3^c & \gamma_4^c \\ 0 & \gamma_1^s & \gamma_2^s & \gamma_3^s & \gamma_4^s \\ d & \gamma_2^c & \gamma_4^c & c_\vartheta & \gamma_3^c \\ 0 & \gamma_2^s & \gamma_4^s & \gamma_1^s & \gamma_3^s \\ c & c & c & c & c \end{pmatrix} \tag{11}$$

In the above equations the matrix entries are functions of the motor parameters and can be found as $c_1 = L_s L_r - L_M^2$, $c_2 = L_r/c_1$, $c_3 = 1/L_{ls}$, $c_4 = L_M/c_1$, $a_2 = -R_s c_2$, $a_3 = -R_s c_3$, $a_4 = -L_M c_4 \omega_r$, $a = 4/5$, $b = -1/5$, $c = -b$, $d = 2/5$, $\gamma_h^c = \cos h\vartheta$, $\gamma_h^s = \sin h\vartheta$ and $\vartheta = 2\pi/5$.

The MPC technique, considering a one-sample time delay for the computations, is as follows. The VSI state at time k constitutes the control action $u(k+1)$. The optimal value is found as a minimization problem in which index J includes several objectives. In particular, deviations of stator currents from their references is penalized in the index or cost function. This is expressed as $J = \|i^*(k+2) - \hat{i}(k+2)\|^2$. Here, symbol $\hat{}$ is used to denote predictions obtained from the model.

2.4. Figures of Merit

The quality of drive control is typically measured using some figures of merit. Here three figures of merit are selected. They are related to the behavior of the system after a step change in the reference for mechanical speed (ω^*). All three figures of merit are obtained from experimental results during transients.

The first indicator (γ_1) is the overshoot, that can be computed as follows:

$$\gamma_1 = 100 \cdot \frac{\max\limits_{k \geq 0} \omega(k) - \omega^*}{\omega^*} \tag{12}$$

The rise time constituted the figure of merit γ_2. This is experimentally obtained measuring the time needed for the drive to evolve from the initial speed to the new reference value. Without loss of generality, one can suppose the step time to correspond to the discrete time index $k = 0$, the initial speed to be $\omega = 0$ and the initial reference to be null, then

$$\gamma_2 = \underset{k \geq 0}{\operatorname{argmin}} \left(\omega^* - \omega(k) \right) \tag{13}$$

Finally, the torque ripple is the root mean squared (RMS) value of the deviation of the actual torque from its reference value T^*

$$\gamma_3 = \sqrt{\frac{1}{N} \sum_{j=k}^{k-N} \left(T^*(j) - T(j) \right)^2}. \tag{14}$$

For clarity, a vector $\Gamma = (\gamma_1, \gamma_2, \gamma_3)$ will be used to refer to all three figures of merit as an ensemble.

3. Experiments

The data for the Pareto analysis are obtained from experimental tests performed in the laboratory testbed described earlier.

3.1. Steady State and Transient Control Results

The results of FSMPC have been featured in many applications including multi-phase drives. In this case, attention must be paid to torque-producing and harmonic subspaces. In sinusoidal steady state one seeks that $\alpha - \beta$ components follow their sinusoidal references and the $x - y$ components be regulated around zero as shown in Figure 3.

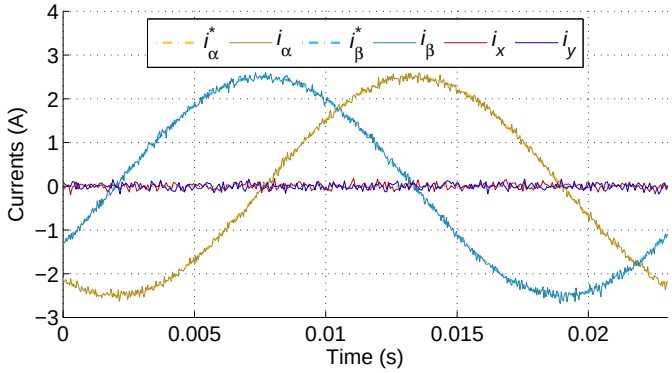


Figure 3. Steady state evolution of currents.

Transient conditions are found for changes in reference speed. A series of step tests will be used for the Pareto analysis. In these tests, the speed set point is changed following a step as shown in Figure 4. For clarity, the case portrayed there corresponds to a start test in which the motor is not running at the start of the test. It is worth pointing out that, in most reports, the only figures of merit considered are derived from speed, including overshoot, rise time, integral absolute error, and integral time absolute error. However, torque ripple is not visible in these figures of merit as seen in Figure 4.

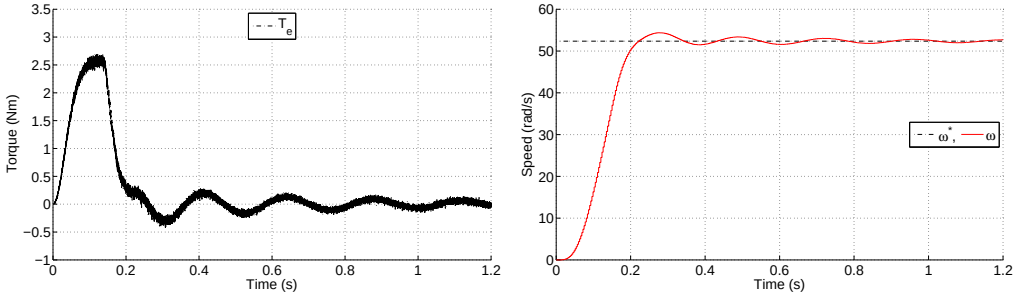


Figure 4. Electrical torque (**left** column) and speed (**right** column) in a step test.

3.2. Pareto Analysis

The Pareto analysis is performed by obtaining experimental values for Γ corresponding to different tunings of the PI. These tunings are obtained as different combinations of the PI gains $(k_p,\ k_i)$. This produces a set of values γ_1, γ_2 and γ_3 for each tuning. For the analysis, a number of PI gains combinations have been considered, where $0 < k_p < 0.5$ and $0 < k_i < 0.02$.

Some of these combinations are not Pareto optimal and must be trimmed. This is performed in the usual way, checking if the Γ values for a particular $(k_p,\ k_i)$ combination A are dominated by some other combination B. Dominated means that at least one value $\gamma_j^B < \gamma_j^A$ with the remaining being at least equal: $\gamma_h^B \leq \gamma_h^A$. These dominant combinations are excluded from the set.

The combinations remaining, after the trimming process, form a set $\boldsymbol{P}$ that can be interpreted as an approximation to the Pareto front. They should lay in a lower dimensional surface as will be shown later. Points in set $\boldsymbol{P}$ are shown in Figure 5 in conjuction with some projections. In those, Γ values are shown in colour. The colour is computed as a linear function of γ_3. The red hue corresponds to higher γ_3, conversely, the blue hue corresponds to lower γ_3. Please note that colour is added just to enhance the 3D perceptions.

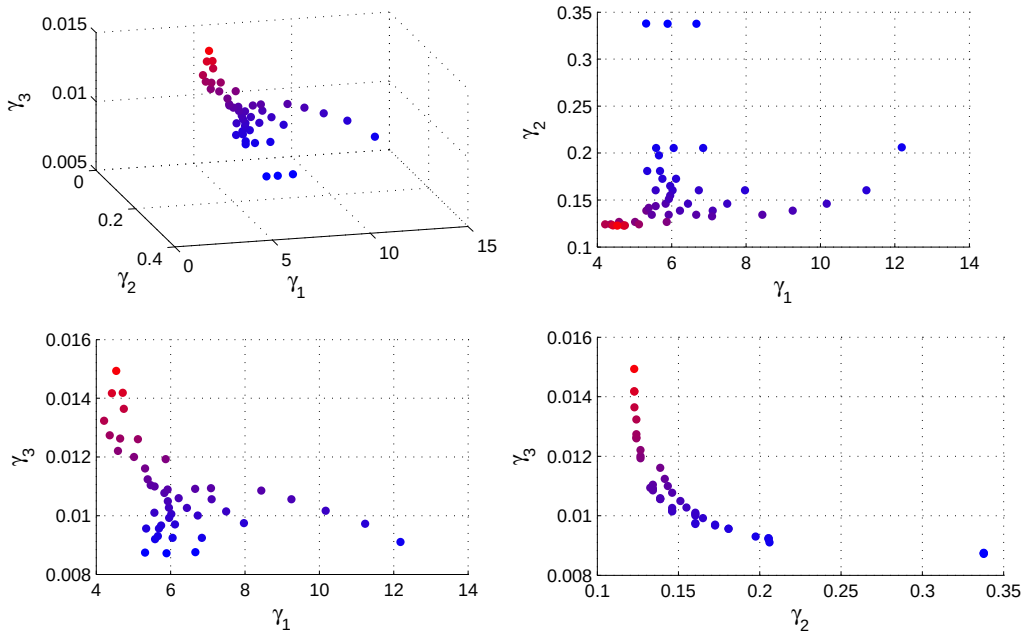


Figure 5. Projections of set $\boldsymbol{P}$ for $\omega^* = 400$ (rpm). Different hues correspond to different γ_3 values.

Points in set $\boldsymbol{P}$ can be shown to be close to a cubic Titeica surface characterized by

$$\gamma_1 \cdot \gamma_2 \cdot \gamma_3 = \overline{\Pi}, \tag{15}$$

where the product of the γ values for each point is a constant $\overline{\Pi}$. In this particular case, a value $\overline{\Pi} = 0.0148$ is found experimentally.

The Pareto front is important in the context of controller tuning because it shows that the performance indicator cannot be improved indefinitely. In fact, the best tunings are those lying in the front because they are the non-dominated combinations.

The trade-offs between performance indicators follow from expression (15). The constraint due to $\gamma_1 \cdot \gamma_2 \cdot \gamma_3$ being constant means that a reduction in γ_1 must produce a higher value for $\gamma_2 \cdot \gamma_3$. This means that either γ_2 or γ_3 or both must increase.

However, these trade-offs, offer flexibility for control tuning. One may choose which figure of merit to prioritize and to what extent. One may be tempted to minimize the distance to the origin as the best tuning. This case corresponds to a set of performance indicators Γ^0 such that

$$\|\Gamma^0\|^2 = \min\left(\gamma_1^2 + \gamma_2^2 + \gamma_3^2\right). \tag{16}$$

The data point Γ^0 is experimentally found as $\gamma_1^0 = 4.30$, $\gamma_2^0 = 0.17$, $\gamma_3^0 = 11.2$. However this solution is, in a general case, just as relevant as the others. This is easily shown considering a change in scale in one performance indicator. Then Γ^0 will move although nothing changes in the physical system. The tuning corresponding to Γ^0 only makes sense if (1) the performance indicators are held as the same importance and (2) they are expressed in units where that equality holds.

In a practical application one may resort to the use of a weighted metric in the γ space. This can be achieved simply by applying scale factors to each performance indicator.

Another aspect that deserves some comments is the existence of limits for tuning. In some publications the proposal is assessed against a previous method resulting in theimprovement of all figures of merit are improved. This is unrealistic unless the previous method is very poorly designed. A proper assessment of any new proposal should use the Pareto front as a way to communicate what aspects are improved [27].

3.3. Variation with Speed

In a practical situation, the actual mechanical speed defines the operation regime of the motor. This variable plays a role in the behaviour of the drive. This means, among other things, that the figures of merit might be different for different speeds.

This can be tested by means of the Pareto analysis being conducted for a different reference ω^*. To do so, the data gathering process is performed again for a different value of ω^*. The results are shown in Figure 6 where $\omega^* = 120$ has been used. In the plot, a different distribution of the Γ values is found. This is further emphasized by Table 2, where different ω^* values are utilized.

Table 2 shows that the reported Γ are for the solution close to the origin (Γ^0). This solution is presented as a way to compare the results for different speeds. The relevance for this solutions can be subjected to the same analysis as in the previous case. Nevertheless, it is interesting to see that the 'optimal' PI tuning depends on the operating mode. This is in contrast with most applications where a single tuning is used for all regimes. In particular, projections $\gamma_1 - \gamma_3$ (lower left) and $\gamma_2 - \gamma_3$ (lower right) show a prominent hyperbola-shaped distribution. This is interesting since γ_3 is not considered in most papers dealing with PI tuning.

A final observation that can be made from Figures 5 and 6 is that the trade-offs are more pronounced in relation with γ_3. This observation is of importance as in some works there is no consideration of different operating regimes.

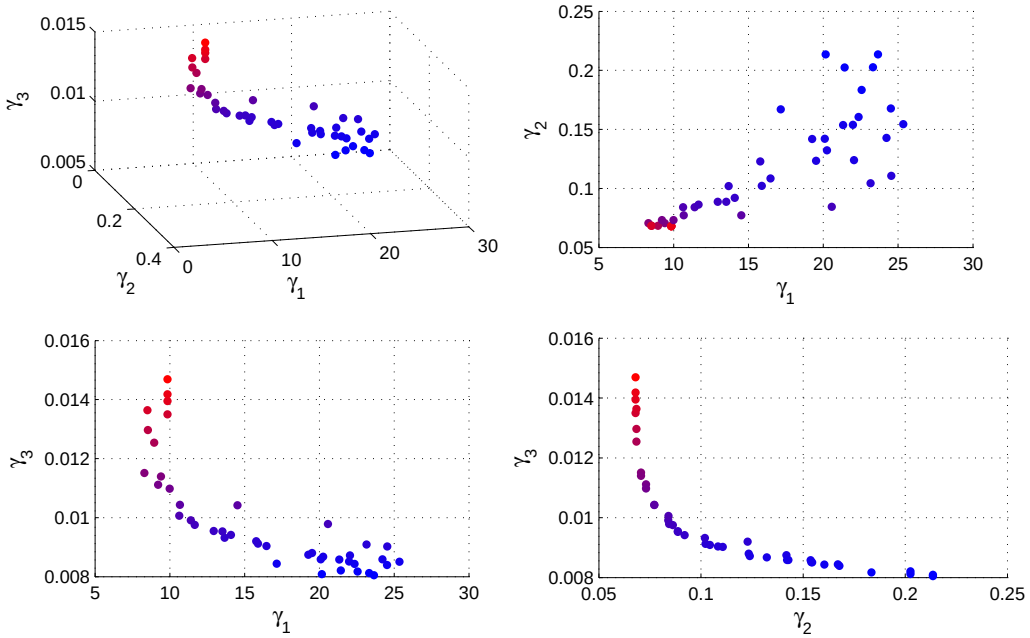


Figure 6. Projections of set $\boldsymbol{P}$ for $\omega^* = 120$ (rpm). Different hues correspond to different γ_3 values.

Table 2. Figures of merit for several speed regimes.

ω^* (rpm)	$k_p^0 \cdot 10^3$ (A/(rad/s))	$k_i^0 \cdot 10^5$ (A/(rad))	γ_1^0 (%)	γ_2^0 (s)	γ_3^0 (mN·m)	$\overline{\Pi}$
400	55	103	4.30	0.17	11.2	8.19
260	96	80	7.11	0.11	12.4	9.70
120	133	58	11.2	0.09	10.3	10.4

4. Discussion

The proposed performance indicators summarize the behavior of the system. The Pareto-optimal tunings pertain to a surface of the lower dimension. In conclusion, any PI tuning must either lie in the surface or be non-optimal. This is in stark contrast to other approaches, where just a handful of configurations are considered and approaches using black-box representations do not provide insight.

Regarding insight, the results of the previous section clearly show the existence of trade-offs between figures of merit considering electro-mechanical variables. The importance of this finding resides in the following points.

1. The interplay between electrical and mechanical variables is made apparent. This relationship is often disregarded in works dealing with PI tuning for variable-speed drives.
2. The existence of limitations in PI tuning is highlighted. The limits are provided by the Pareto front. Without knowing these limits, one could waste time on unfruitful testing.
3. Comparisons between controllers should be made by comparing whole Pareto fronts, instead of particular points. Otherwise one can always present a particular point where one controller outperforms another in some specific figure of merit.

The findings might seem to be negative in nature. After all, there is no known analytical procedure to link controller parameters to performance indicators. Such a procedure would allow for a more systematic, and perhaps automatic, tuning of the PI. However, from the above results, one can derive practices to help PI tuning. In particular, one should prepare to accept that the Pareto frontier cannot be pierced just by using tuning. This has two consequences:

1. For PI tuning, one should instead concentrate on sliding along the surface to obtain the trade-off solution that is best adapted to the particular application.
2. For further improvements, one should concentrate on structural changes either in the control loop or in particular elements: sensors, actuators, etc.

Also, it is worth noting that some figures of merit, such as torque ripple, are commonly not considered in papers dealing with PI tuning. This is something to reconsider since torque ripple plays a crucial role in applications. This omission is, arguably, the result of the lack of tractable models to link electrical and mechanical variables at once.

5. Conclusions

The Pareto analysis presented in the paper show the complexity of PI tuning for drives. However, this result can, be extended to other performance indicators and/or applications. For this, the used methodology does not need to be altered, just included in the new performance indicators in the analysis.

This is in contrast with the common research practice, where assessment of controllers is presented by means of a few cases. Even if the cases are representative, systematic assessment can not be achieved in that way. Instead, the trade-offs between figures of merit should be presented. In this way one can be sure of real improvements compared with just trading one indicator with another.

The relationship between optimal tuning and operating modes must also be reported. Thus, the Pareto analysis must cover all operating modes for the conclusions to gain validity.

In addition, the paper shows that Pareto analysis can be used to improve PI tuning as revealed by the experimental results.

Author Contributions: Conceptualization, M.G.S. and M.R.A.; methodology, M.G.S. and M.R.A.; software, M.G.S. and M.G.O.; validation, M.R.A. and M.G.O.; formal analysis, M.G.S. and M.R.A.; investigation, M.G.S., M.R.A. and M.G.O.; resources, M.R.A.; data curation, M.G.O.; writing—original draft preparation, M.G.S. and M.R.A.; writing—review and editing, M.G.S. and M.G.O.; visualization, M.G.O.; supervision, M.G.S.; project administration, M.R.A.; funding acquisition, M.R.A. All authors have read and agreed to the published version of the manuscript.

Funding: This work is part of grant I+D+i/PID2021-125189OB-I00, with funds by MCIU/AEI/10.13039/501100011033/ by "ERDF A way of making Europe".

Data Availability Statement: The raw data supporting the conclusions of this article will be made available by the authors on request.

Conflicts of Interest: The authors declare no conflicts of interest.

Abbreviations

The following abbreviations are used in this manuscript:

CF	Cost Function
FSMPC	Finite State Model Predictive Control
IFOC	Indirect Field Oriented Control
IM	Induction Machine
PI	Proportional-Integral
PWM	Pulse Width Modulation
RMS	Root Mean Square
VSI	Voltage Source Inverter
WF	Weighting Factors

References

1. Garcia, G.; Stephan, R.M.; Watanabe, E.H. Comparing the indirect field-oriented control with a scalar method. *IEEE Trans. Ind. Electron.* **1994**, *41*, 201–207. [CrossRef]
2. Robyns, B.; Sente, P.A.; Buyse, H.A.; Labrique, F. Influence of digital current control strategy on the sensitivity to electrical parameter uncertainties of induction motor indirect field-oriented control. *IEEE Trans. Power Electron.* **1999**, *14*, 690–699. [CrossRef]
3. Shahid, M.B.; Jin, W.; Abbasi, M.A.; Husain, A.R.B.; Munir, H.M.; Hassan, M.; Flah, A.; Souissi, A.S.E.; Alghamdi, T.A. Model predictive control for energy efficient AC motor drives: An overview. *IET Electr. Power Appl.* **2024**, *18*, 1894–1920. [CrossRef]
4. Bermúdez, M.; Martín, C.; González-Prieto I.; Durán, M.J.; Arahal, M.R.; Barrero, F. Predictive current control in electrical drives: An illustrated review with case examples using a five-phase induction motor drive with distributed windings. *IET Electr. Power Appl.* **2020**, *14*, 1291–1310. [CrossRef]
5. Lim, C.S.; Levi, E.; Jones, M.; Rahim, N.A.; Hew, W.P. FCS-MPC-based current control of a five-phase induction motor and its comparison with PI-PWM control. *IEEE Trans. Ind. Electron.* **2013**, *61*, 149–163. [CrossRef]
6. Bessaad, T.; Benbouali, A.; Taleb, R.; Bouchaib, A. Comparative performance analysis of different controllers for five-phase induction motor drive. *Stud. Eng. Exact Sci.* **2024**, *5*, e11738. [CrossRef]
7. De Wit, P.A.; Ortega, R.; Mareels, I. Indirect field-oriented control of induction motors is robustly globally stable. *Automatica* **1996**, *32*, 1393–1402. [CrossRef]
8. Bazanella, A.S.; Reginatto, R. Robust tuning of the speed loop in indirect field oriented control of induction motors. *Automatica* **2001**, *37*, 1811–1818. [CrossRef]
9. Mossa, M.A.; Vu Quynh, N.; Echeikh, H.; Do, T.D. Deadbeat-Based Model Predictive Voltage Control for a Sensorless Five-Phase Induction Motor Drive. *Math. Probl. Eng.* **2020**, *2020*, 4164526. [CrossRef]
10. Gonzalez-Prieto, A.; González-Prieto, I.; Duran, M.J.; Aciego, J.J. Dynamic response in multiphase electric drives: Control performance and influencing factors. *Machines* **2022**, *10*, 866. [CrossRef]
11. Bugarin, E.; Aguilar-Bustos, A.Y. Position control using an intelligent servomotor in voltage mode and considering friction: Tutorial. *Rev. Iberoam. Autom. Inform. Ind.* **2024**, *22*, 1–12. [CrossRef]
12. Soto-Marchena, D.; Barrero, F.; Colodro, F.; Arahal, M.R.; Mora, J.L. On-Site Calibration of an Electric Drive: A Case Study Using a Multiphase System. *Sensors* **2023**, *23*, 7317. [CrossRef] [PubMed]
13. Shaija, P.; Daniel, A.E. Optimal Tuning of PI Controllers for IM Drive using GWO and TLBO Algorithms. In Proceedings of the 2023 Fifth International Conference on Electrical, Computer and Communication Technologies (ICECCT), Erode, India, 22–24 February 2023; IEEE: Piscataway, NJ, USA, 2023; pp. 1–9.
14. Menghal, P.; Laxmi, A.J. Fuzzy based real time control of induction motor drive. *Procedia Comput. Sci.* **2016**, *85*, 228–235. [CrossRef]
15. Abboud, Y.B.W.; Sbita, L.; Abdelkrim, M. A sensorless neural network speed control of induction motor drive. *Int. J. Signal Syst. Control Eng. Appl* **2008**, *1*, 150–158.
16. Hoggui, A.; Benachour, A.; Madaoui, M.C.; Mahmoudi, M.O. Comparative Analysis of Direct Torque Control with Space Vector Modulation (DTC-SVM) and Finite Control Set-Model Predictive Control (FCS-MPC) of Five-Phase Induction Motors. *Prog. Electromagn. Res. B* **2024**, *108*, 89–104. [CrossRef]
17. Aciego, J.J.; Gonzalez-Prieto, I.; Duran, M.J.; Gonzalez-Prieto, A.; Carrillo-Rios, J. Guiding the Selection of Multi-Vector Model Predictive Control Techniques for Multiphase Drives. *Machines* **2024**, *12*, 115. [CrossRef]
18. Gonçalves, P.; Cruz, S.; Mendes, A. Finite control set model predictive control of six-phase asymmetrical machines—An overview. *Energies* **2019**, *12*, 4693. [CrossRef]
19. Satué, M.G.; Arahal, M.R.; Ramírez, D.R.; Barrero, F. Multi-phase predictive control using two Virtual-Voltage-Vector constellations. *RIAI* **2023**, *20*, 347–354.
20. Zhang, H.; Zhang, Y.; Zhu, Y.; Wang, X. Robust deadbeat predictive current control of induction motor drives with improved steady state performance. *IET Power Electron.* **2023**, *16*, 1281–1292. [CrossRef]
21. Alharbi, A.; Odhano, S.; Smith, A.; Deng, X.; Mecrow, B. A Review of Modeling and Control of Multi-Phase Induction Motors Under Machine Faults. In Proceedings of the 2024 International Conference on Electrical Machines (ICEM), Torino, Italy, 1–4 September 2024; IEEE: Piscataway, NJ, USA, 2024, pp. 1–9.
22. Pancurák, L.; Marcin, D.; Kyslan, K. Sensitivity Analysis of Finite Control Set Model Predictive Direct Speed Control of PMSM. In Proceedings of the 2024 ELEKTRO (ELEKTRO), Zakopane, Poland, 20–22 May 2024; IEEE: Piscataway, NJ, USA, 2024; pp. 1–6.
23. Calderon-Lopez, G.; Villarruel-Parra, A.; Kakosimos, P.; Ki, S.K.; Todd, R.; Forsyth, A.J. Comparison of digital PWM control strategies for high-power interleaved DC–DC converters. *IET Power Electron.* **2018**, *11*, 391–398. [CrossRef]
24. Liu, Y.; Huang, S.; Liao, W.; Liang, G.; Cui, H.; Feng, C.; Wu, X.; Wei, J.; Huang, S. Three-Vector-based Model Predictive Torque Control for Dual Three-Phase PMSM With Torque and Flux Ripples Reduction. *IEEE Trans. Power Electron.* **2024**, *39*, 10009–10020. [CrossRef]

25. Martínez-Luzuriaga, P.N.; Reynoso-Meza, G. Hyper parameter influence in Diferential Evolution based algorithms for PID controller tuning applications. *RIAI* **2023**, *20*, 44–55. [CrossRef]
26. Arahal, M.R.; Barrero, F.; Duran, M.J.; Ortega, M.G.; Martin, C. Trade-offs analysis in predictive current control of multi-phase induction machines. *Control Eng. Pract.* **2018**, *81*, 105–113. [CrossRef]
27. Santis, P.; Sáez, D.; Cárdenas, R.; Núñez, A. Pareto-based modulated model predictive control strategy for power converter applications. *Electr. Power Syst. Res.* **2019**, *171*, 158–174. [CrossRef]
28. Fretes, H.; Rodas, J.; Doval-Gandoy, J.; Gomez, V.; Gomez, N.; Novak, M.; Rodriguez, J.; Dragičević, T. Pareto optimal weighting factor design of predictive current controller of a six-phase induction machine based on particle swarm optimization algorithm. *IEEE J. Emerg. Sel. Top. Power Electron.* **2021**, *10*, 207–219. [CrossRef]

Disclaimer/Publisher's Note: The statements, opinions and data contained in all publications are solely those of the individual author(s) and contributor(s) and not of MDPI and/or the editor(s). MDPI and/or the editor(s) disclaim responsibility for any injury to people or property resulting from any ideas, methods, instructions or products referred to in the content.